

Temporal Action Localization with Multi-temporal Scales

Zan Gao, Member, IEEE, Xinglei Cui, Tao Zhuo, Zhiyong Cheng, An-An Liu, Senior Member, IEEE, Meng Wang, IEEE Fellow, and Shenyong Chen, Senior Member, IEEE, IET Fellow

Abstract -Temporal action localization plays an important role in video analysis, which aims to localize and classify actions in untrimmed videos. The previous methods often predict actions on a feature space of a single-temporal scale. However, the temporal features of a low-level scale lack enough semantics for action classification while a high-level scale cannot provide rich details of the action boundaries. To address this issue, we propose to predict actions on a feature space of multi-temporal scales. Specifically, we use refined feature pyramids of different scales to pass semantics from high-level scales to low-level scales. Besides, to establish the long temporal scale of the entire video, we use a spatial-temporal transformer encoder to capture the long-range dependencies of video frames. Then the refined features with long-range dependencies are fed into a classifier for the coarse action prediction. Finally, to further improve the prediction accuracy, we propose to use a frame-level self attention module to refine the classification and boundaries of each action instance. Extensive experiments show that the proposed method can outperform state-of-the-art approaches on the THUMOS14 dataset and achieves comparable performance on the ActivityNet1.3 dataset. Compared with A2Net (TIP20, Avg{0.3:0.7}), Sub-Action (CSVT2022, Avg{0.1:0.5}), and AFSD (CVPR21, Avg{0.3:0.7}) on the THUMOS14 dataset, the proposed method can achieve improvements of 12.6%, 17.4% and 2.2%, respectively ¹.

Index Terms—Temporal Action Localization; Multi-temporal Scales; Refined Feature Pyramids; Spatial-temporal Transformer; Frame-level Self Attention;

I. INTRODUCTION

In recent years, with the emergence of a large number of Internet videos, Temporal Action Localization (TAL) has attracted lots of attention in academia and industry [38], [33]. As an important branch of video understanding, the goal of TAL is to locate the start and end of each action instance in untrimmed videos and predict the category of actions.

According to different processing strategies, recent TAL methods can be roughly divided into three categories, anchor-based, actionness-guided, and anchor-free methods. The anchor-based methods [13], [8], [46] generate a set of action

proposals with the pre-defined anchors at different temporal scales. Then the actions are classified and the boundaries are regressed. However, due to the fixed pre-defined anchors, the anchor-based methods are not flexible enough for various action categories. Besides, the anchor-based methods are very sensitive to some hyper-parameters. For flexible TAL, the actionness-guided approaches [24], [21], [47], [49], [34], [19], [31] focus on predicting the confidence scores of the start probability, end probability, and duration of action, and then combining them into proposals. Unlike anchor-based methods, actionness-guided approaches do not require pre-defined anchors to generate action proposals. However, such a strategy requires an extra model for action classification, and its computational cost is relatively expensive. Recently, for efficient TAL in videos, the anchor-free strategy [27], [20] only needs to generate a proposal at each temporal position, which is formed by combining the regions from the current position to the start position and end position, and it also does not require the pre-defined anchors. Compared to the actionness-guided methods, anchor-free based methods do not enumerate boundaries, avoiding the redundancy of proposals and reducing the amount of computation.

In order to localize and classify actions with different temporal scales, the majority of existing anchor-free techniques often predict actions on the feature space of a single-temporal scale, *i.e.* feature space of each pyramid layer individually, as illustrated in Figure 1.a. However, the features of a low-level temporal scale lack enough semantics for action classification while a high-level scale cannot provide rich details of action boundaries. As a result, it is difficult to consider both the semantics and boundaries for each action instance simultaneously.

In this paper, we propose a Temporal Action Localization method by using features of Multi-Temporal Scales, namely TAL-MTS. As illustrated in Figure 1.b, to make the feature contain enough semantics and rich details of boundaries, we use the nearest neighbor linear interpolation to merge the semantics information of the high-level temporal features into the low-level. For the Refined Feature Pyramids (RFP), the semantics information from the high-level temporal scale can be passed to the low-level one. Then both the semantics and details of actions can be considered simultaneously. Furthermore, to establish the long temporal scale of the entire video, we propose to use a Spatial-Temporal Transformer (STT) encoder to capture the long-range dependencies of video frames. As illustrated in Figure 1.c, the factorized encoder consists of two transformer encoders in series, a spatial transformer encoder models the latent representation of each video frame, and a temporal transformer encoder models the relationship between frames. Thus, it can represent the spatial-temporal context of

¹Manuscript received July 7th, 2022; This work was supported in part by the National Natural Science Foundation of China (No.61872270, No.62020106004, No.92048301, No.61572357). Young creative team in universities of Shandong Province (No.2020KJN012), Jinan 20 projects in universities (No.2020GXRC0404, No.2018GXRC014).

Z. Gao, X.L Cui (Co-first author), T. Zhuo (Corresponding author) and Z.Y Cheng are with Shandong Artificial Intelligence Institute, Qilu University of Technology (Shandong Academy of Sciences), Jinan, 250014, P.R China.

A.A Liu is with the School of Electrical and Information Engineering, Tianjin University, Tianjin, 300072, China.

M. Wang is with the school of Computer Science and Information Engineering, Hefei University of Technology, Hefei, 230009, P.R China.

S.Y Chen and Z.Gao are with Key Laboratory of Computer Vision and System, Ministry of Education, Tianjin University of Technology, Tianjin, 300384, P.R China.

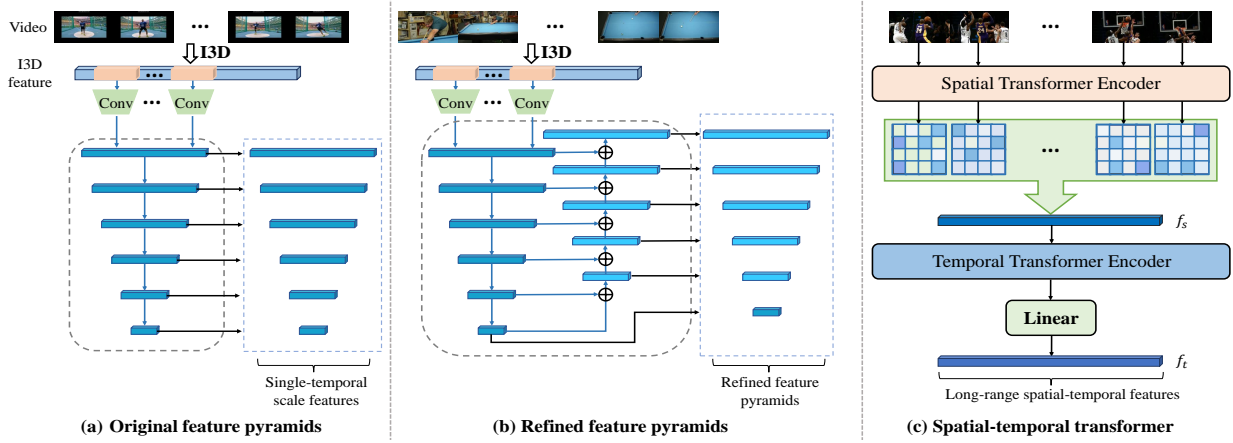


Fig. 1: (a) Original feature pyramids with the single-temporal scale. (b) Refined feature pyramids with multi-temporal scales pass semantics from high-level to low-level scales. (c) Spatial-temporal transformer for long-range dependencies.

the videos at a long-range scale. By combining the refined feature pyramids and long-range spatial-temporal features on the entire video, the proposed method is able to well predict actions with robust features of multi-temporal scales.

In addition, to further enhance the foreground information of video frames, we perform a patch operation on each video frame and use self-attention to extract the relationship between patches to obtain features with salient foreground information. It is able to effectively reduce the influence of background noises on action instances, and enhance the foreground action features inside videos. Extensive experiments show that TAL-MTS achieves 56.9% on MAP@0.5 leading state-of-the-art by 1.8% on THUMOS14 dataset, and achieves comparable results on ActivityNet1.3 dataset.

The main contributions of this paper are summarized as follows:

- We propose a novel temporal action localization with refined features of multi-temporal scales, namely TAL-MTS. Compared to previous approaches, the proposed method is able to provide sufficient semantics, rich details of boundaries, and long-range dependencies for robust temporal action localization.
- We propose to refine the classification and boundaries of action instances with a frame-level self-attention module, which can reduce the noises caused by backgrounds.
- Extensive experiments show that our model outperforms state-of-the-art methods on the THUMOS14 dataset and obtains comparable results on the ActivityNet-1.3 dataset.

The remainder of this paper is organized as follows: Section II introduces related work, and Section III details the proposed TAL-MTS method. In Section IV, the experimental settings are presented, and the results are analyzed on the THUMOS14 dataset and ActivityNet1.3 dataset. In Section V, we present the ablation study. Finally, Section VI presents the conclusions.

II. RELATED WORK

The TAL has become a hot topic in the field of computer vision. More and more researchers have proposed novel methods and achieved good results. In this section, We will introduce

these methods from three aspects anchor-based Localization, anchor-free methods, actionness-guided Localization. At the same time, we will also introduce transformers in computer vision.

Anchor-based Localization. The Anchor-based methods rely on pre-defined anchors of different scales, which are divided into one-stage and two-stage methods. SSAD [22] and GTAN [26] methods are one-stage methods. For the SSAD [22] method, it utilizes a single-shot structure based on 1D convolution to generate anchors for TAL, and GTAN [26] uses 3D ConvNet to extract small segment-level features, and uses temporal Gaussian kernel to generate proposals with different temporal resolutions. About two-stage methods, R-C3D [46] and TALNet [8] are similar to the structure of [29]. R-C3D [46] proposes an end-to-end network that combines candidate segment generation and classification to learn features and accepts input of videos of any length. TALNet [8] expands the receptive field and extracts temporal context for features. Simultaneously, late fusion is used for two-stream architecture. Different from the above two methods, TURN [13] divides the video into equal-length units, and includes extracting unit-level features, classifying action instances, and regressing temporal boundaries. Unlike common anchor-based detection techniques, RCL [42] proposes to use continuous Anchoring representation to achieve high-quality action detection. Confidence scores are regressed from continuous anchor points, and their confidence scores are jointly determined by video features and temporal coordinates. Although these methods can achieve good results, they are not flexible enough and also generate large redundancy.

Anchor-free methods. The anchor-free methods do not require pre-defined anchors, and the action proposal is represented by the distances from the current position to the start position and the end position. Thus there is no need for a large number of hyperparameters, and the computational cost is relatively low. For example, CornerNet [18] uses a convolutional network to generate two sets of heat maps to predict corners for different categories, one for the upper left corner and the other for the lower right corner. And it will also

find the offset positioned by the corner to make the bounding box more accurate. In TAL tasks, SRF-Net [27] designs a Selective Receptive Field Convolution (SRFC) mechanism, which can adaptively adjust the size of the receptive field according to multiple scales of input information at each temporal localization. The AFSD [20] framework consists of three modules: feature extraction, coarse prediction, and refined prediction. It first extracts the pyramid features from the video, then predicts the boundary and classification of the coarse proposal for each pyramid layer, and finally optimizes the boundaries and classification of each proposal through the refined prediction. In addition, A2Net [48] introduces an anchor-free method to solve the problem of too long or too short video sequence length, and it can use the complementary properties to handle temporal sequences of different lengths. In this paper, our method is based on the anchor-free strategy, and we use features of Multi-temporal scales for temporal action localization.

Actionness-guided Localization. This strategy generates proposals by predicting confidence scores for the start probability, end probability, and duration. Different from the anchor-based approach, actionness-guided localization is more flexible in handling action instances that are too long or too short. Earlier in this method, TAG [45] and SSN [52] are proposed. TAG scores the sampled snippets, judges whether it is an action or not, and combines the snippets that are actions into proposals. SSN is based on the TAG method to generate proposals and divides the proposal into three stages: start, end, and activity. Each stage performs a pooling operation and then judges whether the action is complete and the action is classified. Soon after, Lin et al. proposed BSN [24], LGN [23], BMN [21] and BSN++ [34]. BSN first locates the boundaries of temporal action segments and directly combines the boundaries. Then, proposal-level features are extracted based on the sequence of action confidence scores. Based on BSN, LGN proposes a "local to global" approach to jointly learn local and global contexts to generate action proposals, locally locate the accurate proposal boundary and globally evaluate the reliable confidence score. Improved BSN framework to BMN, which densely evaluates the confidence scores of all possible temporal sequences by generating a one-dimensional boundary probability sequence and a two-dimensional BM confidence map. Based on the above frameworks, BSN++ uses a boundary complementary classifier to enrich the context information for boundary prediction, and it designs a proposal relationship module that uses channel-wise and position-wise global dependencies to model proposal-proposal relationships. In addition, PGCN [49] firstly uses graph convolutional networks to capture proposal-proposal relationships. Each proposal is represented as a node, and the two proposals are represented as an edge. Two types of relationships are used, one for capturing the contextual information of each proposal and the other for describing the association between different actions. Similar to PCGN, GTAD [47] uses 3 GCNext modules for feature extraction, gradually aggregating temporal information and multi-level semantics information. Then, the extracted features are fed into the SGAlign layer, and the localization module obtains

the scores of sub-graphs and sorts them, and then gets the final result. Since this method considers all possible combinations of time positions, it requires lots of computational costs.

Transformers in computer vision. The transformer architecture was first proposed in the Natural Language Processing (NLP) task, based on the self-attention mechanism to capture the relationship between sequences. Recently, it has received extensive attention in the field of computer vision, and the self-attention [37] mechanism in the transformer plays an important role in extracting temporal information in videos. For object detection, DETR [5] uses object queries instead of Anchors as candidates. A pure transformer architecture may not be sufficient to model complex temporal dependencies for action detection, Therefore, MS-TCT [10] uses convolutions to promote multiple temporal scales of tokens, and to blend neighboring tokens imposing a temporal consistency. Then, infusing local information between tokens. In the TAL task, ATAG [7] proposes an augmented transformer with an adaptive graph network that captures both long-time and local temporal context information. TAPG [41] designs a unified temporal action proposal generation framework, which consists of a boundary transformer and a proposal transformer, which capture long-term temporal dependencies and enrich the relationship between proposals respectively to predict accurate boundary information and reliable confidence assessment. ViT [11] directly divides the image into patches of the same size and applies the transformer to the image patch sequence, which can well accomplish the task of image classification. Inspired by ViT, we use RFS to enhance the foreground information of the video. The Factorised encoder model in ViViT [1] based on ViT consists of a spatial transformer encoder and a temporal transformer encoder, which models the interactions of different temporal information. Thus, We design STT to extract the long-range spatial-temporal information in the video to enhance the features.

III. OUR APPROACH

Suppose an untrimmed video $V = \{v_i\}_{i=1}^T$ consists of T frames, the set of action instances is represented by $X = \{t_{s,m}, t_{e,m}, \phi_m\}_{m=1}^M$, where s_m and e_m represent the start time and end time, respectively. ϕ_m and M indicate the category of the m -th action instance and the number of action instances in the video, respectively. Our goal is to predict action segments with the start time, end time, and the corresponding action category.

Unlike the previous methods [20], [48], [27] that use the CNN model to exploit the features of single-temporal scale, we propose to use features of multi-temporal scales on videos. Based on an anchor-free TAL framework, our method is able to well locate and classify various actions.

A. Overview

The overview of the proposed method is illustrated in Figure 2. Given a video sequence, we first use I3D to extract features and then refine the feature pyramids by passing semantics from high-level scales to low-level ones, namely Refined

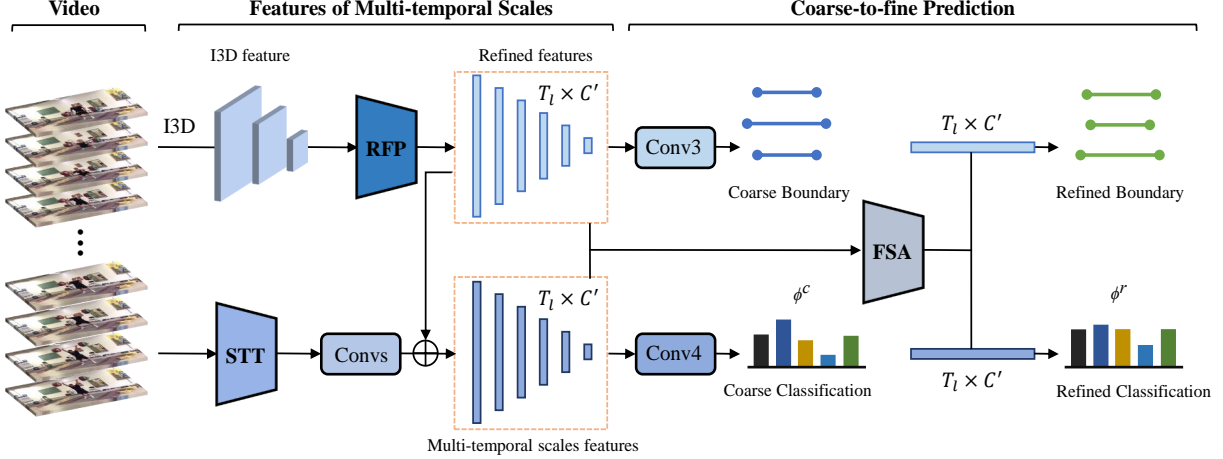


Fig. 2: An overview of the proposed TAL-MTS method. In this architecture, the I3D network is used as the feature extractor. The Refined Feature Pyramids (RFP) produces refined features with stronger semantics information at different temporal scales. The Spatial-Temporal Transformer (STT) excavates the spatial-temporal information of videos. The coarse-to-fine prediction is designed to minimize influence of video background noises, which consists of an Frame-level Self Attention (FSA) module. Note that \oplus is concatenation.

Feature Pyramids (RFP) module. Besides, we use a Spatial-Temporal Transformer (STT) module to capture the long-range dependencies of video frames. Then, by combining the features from RFP and STT, features of multi-temporal scales can be generated for the coarse action prediction. Finally, a Frame-level Self Attention (FSA) module is used to extract the salient foreground information, which further refines the action classification and boundaries (Section. 3.3). Next, we will describe the main modules of the proposed method.

B. Features of Multi-temporal Scales

The features of multi-temporal scales are generated from a Refined Feature Pyramids (RFP) module and a Spatial-Temporal Transformer (STT) module. Details of these two modules are as follows.

Refined Feature Pyramids (RFP). We use the I3D [6] model pre-trained on the Kinetics dataset for both RGB frames and optical flows to obtain I3D features. For a video $V \in R^{C \times T \times H \times W}$, C is the number of channels, T is the temporal duration, H and W are the height and width of the video frame, respectively. The spatial-temporal features are denoted as $\mathbb{F} \in R^{C' \times T' \times H' \times W'}$ through the I3D network, where C' , T' , H' and W' also represent channel, temporal duration, height and width respectively. Then, the spatial-temporal features are converted into a 1D feature space $\mathbb{F}_{st} \in R^{C' \times T'}$ through 3D convolutions, and by downsampling with 1D convolution layers, following [20], the feature pyramids with 6 different temporal scales are generated. Meanwhile, the dimension is 512 for the feature pyramids. The first two temporal scales use 3D convolution downsampling with the kernel of [1, 6, 6] and [1, 3, 3] respectively. The remaining four temporal scales are downsampled using four identical 1D convolutions with kernel = 3 and stride = 2.

Inspired by the previous method [39], we designed a RFP to compensate the semantics information to 1D feature se-

quences and expand the receptive field. To be specific, we add the semantics information of higher-level features to the lower-level features. Then, the features of different temporal scales with stronger semantics information can be obtained. Additionally, different from other similar structures, RFP uses nearest neighbor linear interpolation instead of convolution in the refined feature pyramids process. Thus, there is no need to update the parameters, which reduces the number of trainable parameters and speeds up the calculation. Based on RFP, refined feature pyramids with stronger semantics information $f \in R^{T_i \times C'}$, $T_i \in \{2, 4, 8, 16, 32, 64\}$ can be generated, where T_i represents the different temporal spans. Moreover, a frame-level feature $f_a^c \in R^{T \times C'}$ is generated by taking the feature of the lowest layer into a feature with temporal span T adopting linear interpolate, which is used for further prediction refinement.

Spatial-Temporal Transformer (STT). The long-range dependencies are important for the TAL task. Although we have got the refined feature pyramids at different temporal scales, the long-range spatial-temporal information is still lost because the downsampling using convolution has lower temporal receptive fields from video to spatial-temporal features. Therefore, we use an STT module to extract the long-range dependencies of video frames.

Inspired by ViViT [1], we extract the long-range spatial-temporal information of videos with a factorised encoder, which consists of a spatial transformer encoder and a temporal transformer encoder in series. The spatial transformer encoder excavates the relationship within video frames from the same temporal index. Then, all the spatial feature outputs after temporal embedding are used as the input for the temporal transformer encoder. The temporal encoder connects the frames with different temporal indexes for capturing the temporal information, and we will obtain features with long-range spatial-temporal information from STT. Therefore, the

long-range spatial-temporal information is supplemented to the output of the refined feature pyramids.

Specifically, our method employs Multi-Headed Self Attention (MSA) [37] in parallel, and Layer Normalisation (LN) [2] is applied before each MSA block. We first embed spatial position encoding for video $V = \{v_i\}_{i=1}^T$ and feed into the spatial transformer encoder and get a feature sequence f_s . Then, we embed temporal information to this feature sequence and take the feature into the temporal transformer encoder. Finally, feature $f_t \in R^{T_j \times C'}$ with long-range spatial-temporal information at one temporal scale is produced, where T_j is temporal scale and C' is channel. Therefore, this process is denoted as follows:

$$\begin{aligned} f_s &= \text{MSA}(\text{LN}(v_i)) \quad i = 1, \dots, T, \\ f_t &= \text{Linear}(\text{MSA}(\text{LN}(f_s))), \end{aligned} \quad (1)$$

where T represents the number of frames in the video and $\text{Linear}(\cdot)$ represents the fully connected layer. In order to gain multi-scale features with long-range spatial-temporal information, we downsample f_t through multiple 1D convolutions to produce feature sequences $f_l \in R^{T_l \times C'}$ at different temporal scales, $T_l \in \{2, 4, 8, 16, 32, 64\}$. Then, we followed by concatenating the feature sequences f obtained by RFP and the feature sequences f_l to produce features of multi-temporal scales f_{mts} , which is represented by:

$$f_{mts} = [f, f_l], \quad (2)$$

where $[\cdot]$ indicates the concatenation. We project features of multi-temporal scales and refined feature pyramids to f_{cls} and f_{loc} respectively in two 1D convolutions at each temporal scale, which is computed as follows:

$$\begin{aligned} f_{loc} &= \text{Conv1}(f), \\ f_{cls} &= \text{Conv2}(f_{mts}), \end{aligned} \quad (3)$$

f_{loc} for localization and f_{cls} for classification of action instances. Two 1D convolutions have the same kernel and stride.

C. Coarse-to-fine Prediction

Based on the refined features of multi-temporal scales, coarse prediction results can be obtained with a classifier. To further improve the performance, we propose to use a Frame-level Self Attention (FSA) module for both the action category and boundary refinement.

Coarse Prediction. Based on f_{loc} and f_{cls} , we use the two 1D convolutions to produce coarse start and end boundary distances (d_n^s, d_n^e), and coarse class score ϕ_n^c , respectively, which are computed as following:

$$\begin{aligned} d_n^s &= \text{Conv3}(f_{loc}), \\ d_n^e &= \text{Conv3}(f_{loc}), \\ \phi_n &= \text{Conv4}(f_{cls}), \end{aligned} \quad (4)$$

where n represents position in the different temporal scales and d_n^s represents the distance from position n to the start time, and d_n^e represents the position from position n to the end time. Then, the coarse boundaries ($t_{s,n}^c, t_{e,n}^c$) can be inferred, where $t_{s,n}^c$ and $t_{e,n}^c$ represent the coarse starting and ending time of

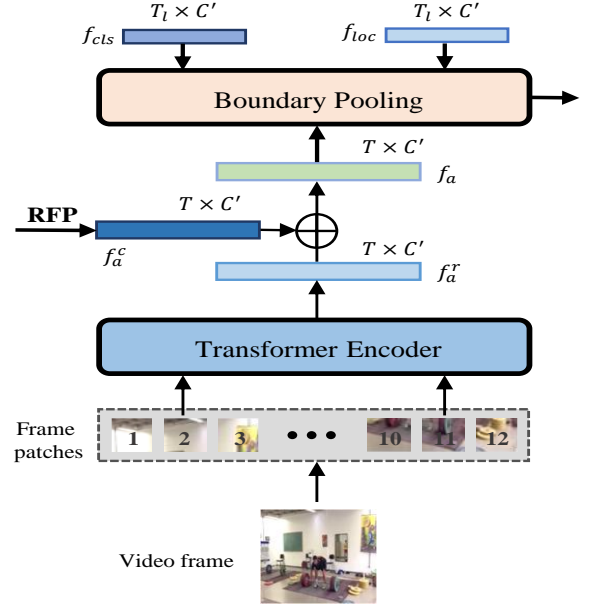


Fig. 3: Frame-level Self Attention (FSA) module. The entire video frame is divided into frame patches and embedded with position encoding, and feed into the Transformer Encoder to generate f_a^r . Then, combined with f_a^c from RFP module to produce f_a . Finally, taking features f_{loc} and f_{cls} from coarse prediction and f_a into the Boundary Pooling and obtaining features of fine-grained.

the corresponding n -th location in refined pyramid features and $n \in \{0, 1, 2, \dots, T_l - 1\}$.

Frame-level Self Attention (FSA). As the features of pyramid go deeper, the temporal dimension will become small and it is difficult to find accurate boundaries. Therefore, we use the frame-level feature for boundary pooling [20]. Since frame-level features are derived from the lowest level of feature pyramids, they ignore the influence of internal background noises in each video frame. Thus, we use a self-attention [37] mechanism to minimize this influence. Inspired by ViT [11], we propose to use a Frame-level Self Attention (FSA) module to process the image of each frame, which maximizes the separation of foreground and background noises.

As illustrated in Figure 3, we take all video frames as input of a transformer encoder and divide each video frame $v_i \in R^{H' \times W' \times C'}$ into frame patches. Then, the relationship between patches in each frame can be built. Specifically, we divide the frame of $H' \times W' \times C'$ into patches $v_{i,z}$ with the size of $D \times D$ where $z \in \{1, 2, \dots, Z\}$ and concatenate Z patches into vectors that embedded patches positional encoding. Next, vectors will be fed into the transformer encoder, which consists of an MSA and an LN block. Finally, based on the outputs of the transformer encoder, we use the fully connected layer to get a frame-level feature to represent the foreground information, which is denoted as:

$$\begin{aligned} v_{i,z} &= \text{TP}(v_i) \quad i = 1, \dots, T, \\ f_a^r &= \text{MSA}(v_{i,z} + \text{PE}(v_{i,z})), \quad z = 1, \dots, Z, \end{aligned} \quad (5)$$

where $\text{PE}(\cdot)$ represents patches position embedding for each

video frame and $\text{TP}(\cdot)$ stands for dividing video frames into patches. Frame-level features for refined prediction from f_a^c generated by RFP and f_a^r obtained by FSA. We concatenate f_a^c and f_a^r for refined frame-level feature f_a . Then, we take the features f_{cls} and f_{loc} in the coarse prediction and the frame-level feature f_a in the fine prediction into boundary pooling [20]. The features of fine-grained f_{loc}^r and f_{cls}^r are defined as follows:

$$\begin{aligned} f_{loc}^r &= \text{BP}(f_{loc}, f_a), \\ f_{cls}^r &= \text{BP}(f_{cls}, f_a), \end{aligned} \quad (6)$$

where BP is a boundary pooling method [20]. Fine-grained prediction for f_{loc}^r and f_{cls}^r are produced by two different 1D convolution layers respectively. Specifically, one convolution layer is used to predict the offsets $(\Delta t_{s,n}^r, \Delta t_{e,n}^r)$ for boundary regression, and the other is used to predict refined class score ϕ^r . Finally, we add the offsets of boundaries $(\Delta t_{s,n}^r, \Delta t_{e,n}^r)$ to coarse boundary and get the refined boundaries $(t_{s,n}^r, t_{e,n}^r)$.

D. Training and Inference

Training. The set of action instances predicted by coarse prediction and refined prediction contains N samples, which is larger than the maximum number of ground-truth action instances in the dataset. TAL-MTS uses multiple losses for the coarse boundary regression and classification and the binary cross-entropy loss is used for the probability of the proposal. The computation of our total loss function can be denoted by

$$L = L_{cls}^c + L_{cls}^r + \alpha(L_{loc}^c + L_{loc}^r) + \beta L_{bce}, \quad (7)$$

where L is the total loss, L_{cls}^c and L_{cls}^r are the loss of the coarse classification and refined classification, respectively. L_{loc}^c and L_{loc}^r are the loss of the coarse boundary regression and refined boundary regression, respectively. L_{bce} is the loss of binary cross-entropy [20]. α and β are hyper-parameters. For the coarse classification, focal loss [25] is applied as the constraint, because it can not only adjust the weight of positive and negative samples but also control the weight of difficult and easy classification samples, which is computed as follows:

$$L_{cls}^c = \frac{1}{N^c} \sum_{n=1}^{N^c} L_{\text{focal}}(\phi_n^c, \phi_n), \quad (8)$$

where N^c is the number of the positive samples in the coarse process, it is regarded as a positive sample when it is located in the ground truth samples. ϕ_n^c is the coarse classification results and ϕ_n is the ground truth labels. For the refined classification, we use a focal loss as,

$$L_{cls}^r = \frac{1}{N^r} \sum_{n=1}^{N^r} L_{\text{focal}}(\phi_n^r, \phi_n), \quad (9)$$

where N^r is the number of the positive samples when the coarse proposals have a tIoU higher than 0.5 with ground truth samples. ϕ_n^r is the refined classification results predicted and ϕ_n is the ground truth labels. We adopt GIoU loss [30] as the constraint for coarse boundary regression, which is computed as follows:

$$L_{loc}^c = \frac{1}{N^c} \sum_{n=1}^{N^c} (1 - \text{GIoU}(\psi_n^c, \psi_n)), \quad (10)$$

where $\psi_n^c = (t_{s,n}^c, t_{e,n}^c)$ is the coarse boundaries predicted by the coarse process, and $\psi_n = (t_{s,n}, t_{e,n})$ is the corresponding ground truth. For the refined boundary regression, we use Smooth L1 loss [14] as loss function and can be calculated as:

$$L_{loc}^r = \frac{1}{N^r} \sum_{n=1}^{N^r} \left(\text{smooth}_{L1}(\hat{\Delta}_n, \Delta_n) \right), \quad (11)$$

where $\hat{\Delta}_n = (\Delta t_{s,n}^c, \Delta t_{e,n}^c)$ is the offset between the coarse boundaries and the corresponding ground truth. $\Delta_n = (\Delta t_{s,n}^r, \Delta t_{e,n}^r)$ is the regression targets of our refined process. In addition, we use the binary cross-entropy loss to suppress proposals with low quality, which is defined as:

$$L_{bce} = \frac{1}{N^r} \sum_{n=1}^{N^r} \text{BCE} \left(\varepsilon_n, \frac{|\psi_n^r \cap \psi_n|}{|\psi_n^r \cup \psi_n|} \right), \quad (12)$$

where BCE is the binary cross-entropy loss. ψ_n^r and ψ_n are the refined boundaries and the corresponding ground truth, respectively. ε_n is the location.

Inference. In the inference stage, we use the coarse boundaries (t_s^c, t_e^c) , coarse classification results ϕ^c , the offsets from refined process $(\Delta t_s^r, \Delta t_e^r)$, refined classification results ϕ^r and confidence scores ε by our network. The final prediction for each clip can be computed as:

$$\begin{aligned} t_{s,n}^p &= t_{s,n}^c + \frac{1}{2} d_n^c \Delta t_{s,n}^r, \\ t_{e,n}^p &= t_{e,n}^c + \frac{1}{2} d_n^c \Delta t_{e,n}^r, \\ \phi_n^p &= \frac{1}{2} (\phi_n^c + \phi_n^r) \varepsilon_n, \end{aligned} \quad (13)$$

where the $d_n^c = t_{e,n}^c - t_{s,n}^c$. Finally, we adopt Soft-NMS [4] to process all predictions to suppress redundant proposals.

IV. EXPERIMENTS

A. Datasets

To verify the effectiveness of our proposed method, we conduct experiments on two benchmark datasets.

THUMOS14 [16] dataset contains 1010 validation videos and 1574 testing videos with 101 action categories. We follow the [16], 200 untrimmed videos in the validation set and 213 untrimmed videos in the test set are used for training and testing, respectively. These videos contain 20 categories labeled for temporal action localization. Each video has more than 15 action annotations.

ActivityNet1.3 [15] dataset contains 19,994 untrimmed videos with 200 action categories. We follow the setting in [15] and divide the dataset into training, testing and validation with a ratio of 2:1:1. There are around 1.5 action instances for each video.

B. Experimental Settings

Parameters. In our experiments, we follow the experimental setup of [20]. On the THUMOS14 dataset, we sample RGB and optical flow frames using a frame rate of 10 frames per second (fps) and split the video into clips. For each clip, we set its length T to 256 frames, and adjacent clips will have

TABLE I: Performance comparison with state-of-the-art methods on THUMOS14 dataset measured by mAP with different tIoU thresholds. The bold numbers represent the best performance.

Type	Methods	Backbone	0.1	0.2	0.3	0.4	0.5	0.6	0.7	Avg {0.1:0.5}	Avg {0.3:0.7}
Anchor-based	SSAD [22]	TS	50.1	47.8	43.0	35.0	24.6	-	-	40.1	-
	TURN [13]	C3D	54.0	50.9	44.1	34.9	25.6	-	-	41.9	-
	R-C3D [46]	C3D	54.5	51.5	44.8	35.6	28.9	-	-	43.1	-
	CBR [12]	TS	60.1	56.7	50.1	41.3	31.0	19.1	9.9	47.8	30.3
	TALNet [8]	I3D	59.8	57.1	53.2	48.5	42.8	33.8	20.8	52.3	39.8
	GTAN [26]	P3D	69.1	63.7	57.8	47.2	38.8	-	-	55.3	-
	PCG-TAL [35]	I3D	71.2	68.9	65.1	59.5	51.2	-	-	63.2	-
Actionness	CDC [31]	-	-	-	40.1	29.4	23.3	13.1	7.9	-	22.8
	SSN [52]	TS	60.3	56.2	50.6	40.8	29.1	-	-	47.4	-
	TAG [45]	TS	64.1	57.7	48.7	39.8	28.2	-	-	47.7	-
	BSN [24]	TS	-	-	53.5	45.0	36.9	28.4	20.0	-	36.8
	BMN [21]	TS	-	-	56.0	47.4	38.8	29.7	20.5	-	38.5
	DBG [19]	TS	-	-	57.8	49.4	42.8	33.8	21.7	-	41.1
	GTAD [47]	TS	-	-	54.5	47.6	40.2	30.8	23.4	-	39.3
	BSN++ [34]	TS	-	-	59.9	49.5	41.3	31.9	22.8	-	41.1
	BU-TAL [51]	TS	-	-	53.9	50.7	45.4	38.0	28.5	-	43.3
	TCA-Net [28]	TS	-	-	60.6	53.2	44.6	36.8	26.7	-	44.4
	RTD-Action [36]	TS	-	-	68.3	62.3	51.9	38.8	23.7	-	49.0
	RCL [42]	TS	-	-	70.1	62.3	52.9	42.7	30.7	-	51.7
	DCAN [9]	TS	-	-	68.2	62.7	54.1	43.9	32.6	-	52.3
Others	SCNN [32]	-	47.7	43.5	36.3	28.7	19.0	-	-	19.0	-
	GTAD+PGCN [47]	TS	-	-	66.4	60.4	51.6	37.6	22.9	-	47.8
	ContextLoc [53]	I3D	-	-	68.3	63.8	54.3	41.8	26.2	-	50.9
	Sub-Action [38]	I3D	66.1	60	52.3	43.2	32.9	-	-	50.9	-
	VSGN [50]	TS	-	-	66.7	60.4	52.4	41.0	30.4	-	50.2
Anchor-free	A2Net [48]	I3D	61.1	60.2	58.6	54.1	45.5	32.5	17.2	55.9	41.6
	SRF-Net [27]	C3D	-	-	56.5	50.7	44.8	33.0	20.9	-	41.2
	AFSD [20]	I3D	-	-	67.3	62.4	55.5	43.7	31.1	-	52.0
	TAL-MTS (Ours)	I3D	75.3	73.8	70.5	65.0	56.9	46.0	32.7	68.3	54.2

temporal overlap, which is set to 30 in training and 128 in testing. On the ActivityNet1.3 dataset, the frames are sampled by different fps, we guarantee that the number of each video frame is 768. On both datasets, we set the size of each frame to 96×96 and the size of frame patches D to 24. We also use random crop, and horizontal flipping as the data augmentation during training.

We use Adam [17] optimizer for model training and the epochs are set to 25. Besides, the learning rate is 10^{-5} , the weight decay is 10^{-3} , and the batch size is set to 1. The hyperparameters are empirically defined as $\alpha = 10$ and $\beta = 1$ on THUMOS14 dataset. On the ActivityNet1.3 dataset, $\alpha = 1$ and $\beta = 1$. In addition, the tIoU threshold in Soft-NMS [4] is set to 0.3 for THUMOS14 and 0.85 for ActivityNet1.3, respectively.

Evaluation metrics. In the TAL task, the mean Average Precision (mAP) is used as the evaluation metric. We report mAP for all experiments. Besides, the tIoU thresholds are [0.1 : 0.1 : 0.7] for THUMOS14 and [0.5 : 0.05 : 0.95] for ActivityNet1.3.

C. Comparison with state-of-the-art methods

We compare the proposed TAL-MTS method with several state-of-the-art methods, which contain anchor-based, actionness-guided, anchor-free, and other approaches. Table I and Table II report the comparison results on THUMOS14

and ActivityNet1.3 dataset, respectively. Then we discuss the results as follows.

Results on THUMOS14. Table I reports the comparison results on the THUMOS14 dataset. For some methods, their tIoU thresholds of 0.1 and 0.2 or 0.6 and 0.7 are not reported. Therefore, we report $Avg\{0.1 : 0.5\}$ and $Avg\{0.3 : 0.7\}$, which are represent the average mAP for all tIoU thresholds $\{0.1 : 0.1 : 0.5\}$ and $\{0.3 : 0.1 : 0.7\}$, respectively. Our method outperforms strong opponents AFSD, RTD-Action, RCL, DCAN and ContextLoc for all thresholds on $Avg\{0.3 : 0.7\}$, and exceeded 2.3%, 5.2%, 2.5%, 1.9% and 3.3%, respectively. For the $Avg\{0.1 : 0.5\}$, the TAL-MTS method outperforms PCG-TAL and A2Net by 5.1% and 12.4%, respectively. These results show that our performance significantly outperforms the current state-of-the-art methods, and the TAL-MTS method improves from 55.5% to 56.9%, when the threshold is 0.5. At the threshold 0.6, the TAL-MTS method exceeds DCAN method 2.1%, the TAL-MTS method is slightly improved compared with DCAN for thresholds 0.7. Especially when the threshold is 0.4, the TAL-MTS method is more than 2% higher than state-of-the-art methods. TAL-MTS method is only 0.4% higher than the latest RCL method at threshold 0.3. For thresholds 0.1 and 0.2, the TAL-MTS method is more than 3% than PCG-TAL and more than 13% better than A2Net. Although A2Net and AFSD are anchor-free methods, A2Net leverages the advantages of

anchor-base and anchor-free and AFSD focuses on refining the boundaries with a saliency-based refinement module, which ignores the importance of enough semantics and long-range spatial-temporal information. In TAL-MTS, features of multi-temporal scales with this information are used for TAL. From the above discussion results, we can see that we have the best results for all tIoU thresholds. Therefore, for anchor-based, anchor-free, etc. methods, the TAL-MTS method outperforms these methods by a large margin at all tIoU thresholds.

TABLE II: Performance comparison with state-of-the-art methods on ActivityNet1.3 dataset measured by mAP at different tIoU thresholds.

Type	Methods	0.5	0.75	0.95	Avg
Anchor-based	R-C3D [46]	26.8	-	-	-
	TALNet [8]	38.2	18.3	1.3	20.2
	GTAN [26]	52.6	34.1	8.9	34.3
	PCG-TAL [35]	44.3	29.9	5.5	28.9
Actionness	CDC [31]	45.3	26.0	0.2	23.8
	SSN [52]	43.2	28.7	5.6	28.3
	TAG [45]	41.1	24.1	5.0	24.9
	BSN [24]	46.5	30.0	8.0	30.0
	BMN [21]	50.1	34.8	8.3	33.9
	GTAD [47]	50.4	34.6	9.0	34.1
	BC-GNN [3]	50.6	34.8	9.4	34.3
	BSN++ [34]	51.3	35.7	9.0	34.9
	BU-TAL [51]	43.5	33.9	9.2	30.1
	RTD-Action [36]	47.2	30.7	8.6	30.8
	TCA-Net[BMN] [28]	52.3	36.7	6.9	35.5
Others	PGCN [49]	48.3	33.2	3.3	31.1
	ContextLoc [53]	56.0	35.2	3.6	34.2
	VSGN [50]	52.3	35.2	8.3	34.7
	Sub-Action [38]	37.1	24.1	5.8	24.1
Anchor-free	A2Net [48]	43.6	28.7	3.7	27.8
	AFSD [20]	52.4	35.3	6.5	34.4
	TAL-MTS (Ours)	52.4	34.7	6.0	34.1

Results on ActivityNet1.3. Table II shows the comparison results on the ActivityNet1.3 dataset, where *Avg* indicates the average mAP for all tIoU thresholds {0.5:0.05:0.95}. TAL-MTS method can obtain comparable results with other state-of-the-art methods on the ActivityNet1.3 dataset. Because the action instances in the ActivityNet1.3 dataset are long and the scenes where some actions occur are discontinuous, it is very challenging for the anchor-free based methods to detect all the action instances. Thus, most TAL methods cannot achieve the best performance on both datasets simultaneously. For example, RTD-Action can achieve better performance on the THUMOS14 dataset and the result is 49.0% for $Avg\{0.3 : 0.7\}$, but only 30.8% on the ActivityNet1.3 dataset. Similarly, BSN++ achieves 34.9% on the ActivityNet1.3 dataset, but it is inefficient on the THUMOS14 dataset and the result only is 41.1% for $Avg\{0.3 : 0.7\}$. The reason for this phenomenon is that the temporal difference between the THUMOS14 dataset and the ActivityNet1.3 dataset is huge. At the same time, it can be seen that TCA-Net achieves the best results on the anet dataset, which is 1.4% higher than our method, but 9.8% lower than TAL-MTS on the THUMOS14 dataset. Because the feature extraction method we use on the ActivityNet1.3 dataset is different from TCA-Net, the feature extraction method of

TSN [44] adopted by TCA-Net often performs better on the ActivityNet1.3 dataset than the I3D [6] method. Therefore, some methods can perform well on the THUMOS14 dataset but poorly on the ActivityNet1.3 dataset, and vice versa. From Table II, it can be seen that the actionness-guided methods are more suitable for the ActivityNet1.3 dataset, and they are more likely to obtain better performance. In addition, ContextLoc is a strong opponent on THUMOS14 dataset, which is 3.3% lower than TAL-MTS for $Avg\{0.3 : 0.7\}$. But on the ActivityNet1.3 dataset, it is only 0.1% higher than ours. Similar to ContextLoc, Comparing TAL-MTS with GTAD has the same result on the ActivityNet1.3 dataset, but TAL-MTS is 14.9% higher than GTAD on the THUMOS14 dataset for $Avg\{0.3 : 0.7\}$. For the GTAN, our method is 13% higher than it on the THUMOS14 dataset for $Avg\{0.1 : 0.5\}$. Yet, TAL-MTS only is 0.2% lower than GTAN on the ActivityNet1.3 dataset. Thus, although the proposed TAL-MTS method does not achieve the best results, its performance is still competitive. From the above experimental analysis, it can be concluded that our method has good generalization ability.

Inference time. We compare the inference speed between TAL-MTS and other methods on the THUMOS14 dataset. Our model is evaluated on a Tesla V100 GPU, its speed of inference is 1824 fps. As shown in Table III, TAL-MTS is fast and the speed of inference reached second place. Our method is slower than AFSD because of two aspects. First, we use a transformer to excavate spatial-temporal information between frames. Next, we divide each frame of the video into patches and pass each patch through the self-attention mechanism. These require a higher computational cost. Nevertheless, TAL-MTS is still efficient.

TABLE III: Comparison of inference time on THUMOS14 dataset.

Model	GPU	FPS
SCNN[32]	-	60
CDC[31]	TITAN Xm	500
R-C3D[46]	TITAN Xm	569
R-C3D[46]	TITAN Xp	1030
PBRNet[43]	1080Ti	1488
AFSD[20]	1080Ti	3259
AFSD[20]	V100	4057
TAL-MTS (Ours)	V100	1824

V. ABLATION STUDY

To verify the effectiveness of each module in our method, we follow the previous methods [20], [39], [49], [51], [27], [48], [40] to conduct the ablation study on the THUMOS14 dataset and ActivityNet1.3 dataset. We mainly focus on the following aspects: validity of the RGB and optical-flow streams, effects of RFP, STT, and FSA modules, the effect of patch size for FSA, and the impact of different tIoU thresholds, visualization prediction boundaries, and loss convergence analysis.

A. Validity of the RGB and optical-flow streams.

We use both the RGB stream and optical-flow stream for TAL and combine them with an average fusion. To further verify the effectiveness of each stream, we conduct experiments

on the ActivityNet1.3 dataset and THUMOS14 dataset. From Table IV, for ActivityNet1.3 dataset, the RGB stream with Avg is 32.5% and the optical-flow stream with Avg is 32.6%, but the result of fusion is 34.1%. We can observe better results for optical-flow stream at tIoU thresholds of 0.5 and 0.75, and better results for RGB stream at tIoU threshold of 0.95. Similarly, for the THUMOS14 dataset, it can be intuitively seen that the a huge difference between single stream and two-stream results. The RGB stream with $Avg\{0.1 : 0.7\}$ is 50.9% and the optical-flow stream with $Avg\{0.1 : 0.7\}$ is 50.4%, but the result of fusion is 60.0%. From the average of three data, we can be seen that the result of the fusion is 9.1% higher than the RGB stream, and 9.6% higher than the optical-flow stream. Similarly, we can see from the table that RGB and optical-flow streams are complementary. When the temporal tIoU threshold is low, the RGB stream can get better results, and the tIoU threshold is high, the optical-flow stream can get good results. For example, the RGB stream has good performance, and the tIoU threshold is from 0.1 to 0.4. The optical-flow stream is higher than RGB from 0.5 to 0.7. Meanwhile, the dense optical flow field can provide motion information, which is very important for the acquisition of spatial-temporal information. Thus, the two-stream network is more effective in the two datasets.

TABLE IV: Validity of the RGB and optical flow stream on ActivityNet1.3 dataset.

	0.5	0.75	0.95	Avg
RGB	50.1	33.0	6.5	32.5
Flow	51.1	33.4	4.9	32.6
Fusion	52.4	34.7	6.0	34.1

TABLE V: Validity of the RGB and optical flow stream on THUMOS14 dataset.

	0.1	0.2	0.3	0.4	0.5	0.6	0.7	Avg {0.1:0.7}
RGB	66.4	64.7	61.5	55.4	46.9	37.0	24.2	50.9
Flow	62.5	61.0	58.4	54.7	48.6	39.4	28.4	50.4
Fusion	75.3	73.8	70.5	65.0	56.9	46.0	32.7	60.0

B. Effects of RFP, STT, and FSA modules.

To verify the effects of our proposed modules, we evaluate these modules and verify the feasibility of module stacking. In Table VI, the baseline reaches 52.0% on the THUMOS14 dataset. When we add the RFP to refined feature pyramids with semantics information at different temporal scales, the improvement is 0.6%, which shows that the semantics information of features is indispensable for TAL tasks. Besides, we propose an STT to fully excavate spatial-temporal information and generate features with long-range dependencies in the video, which improves the performance by 0.8%. Then, by combining RFP and STT, the features of multi-temporal scales are gained, and the average mAP is further improved by 1.1%. This shows the effectiveness of the proposed two modules, and features of multi-temporal scales are very important for TAL-MTS. Additionally, we use an FSA module for distinguishing

foreground and background, which captures the foreground information inside each frame in the video and reduces noises, and further improves the localization and classification of action instances. By fusing all three modules, the proposed TAL-MTS method achieves the best performance (54.2%) on the THUMOS14 dataset, which outperforms the baseline by 2.2%. Based on the above analysis, it can be seen that our proposed three modules are very effective for TAL tasks.

TABLE VI: Benefits of RFP, STT and FSA on THUMOS14.

baseline	✓	✓	✓	✓	✓
RFP		✓		✓	✓
STT			✓	✓	✓
FSA					✓
Avg {0.3:0.7}	52.0	52.6	52.8	53.1	54.2

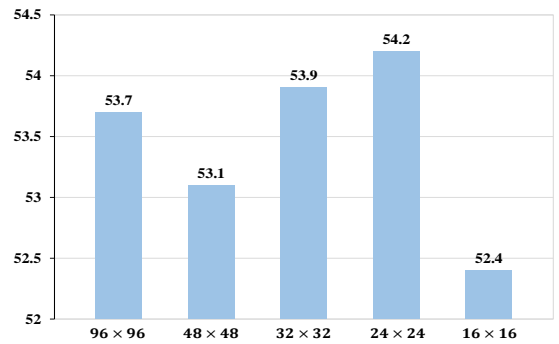


Fig. 4: The average mAP for different patch sizes on the THUMOS14 dataset, where the x-coordinate indicates the patch size, and the y-coordinate denotes $Avg\{0.3 : 0.7\}$.

C. The effect of patch size for FSA.

Because the dividing frame strategy can process each patch, more details can be obtained, which is very important for maximizing the separation of foreground action and background noise. Therefore, we divide all frames of the whole video, and our FSA models the patch of $D \times D$. Because the size of the video frame patches has an impact on separating foreground and background noise, in this section, we discuss the effect of the patch of different sizes on TAL-MTS. As shown in Figure 4, A patch size of 96×96 means that we directly perform self-attention on the original video frame, and we can find that the second-best result is obtained. Because this does not take into account the fine-grained information within each video frame, it can not separate the foreground action and background noise to the greatest extent. On the contrary, when we divide each video frame, we can capture fine-grained information and greatly reduce the impact of background noise. When patch size is set to 24×24 , TAL-MTS has the best results on average. From the figure, we can see that different patch sizes have different results. Thus, we test the patch size from large to small (Note that the patch size must be divided by the size of the video frame), and we find that when the patch size increased from 48×48 to 24×24 , the effect was steadily improving. But the effect becomes

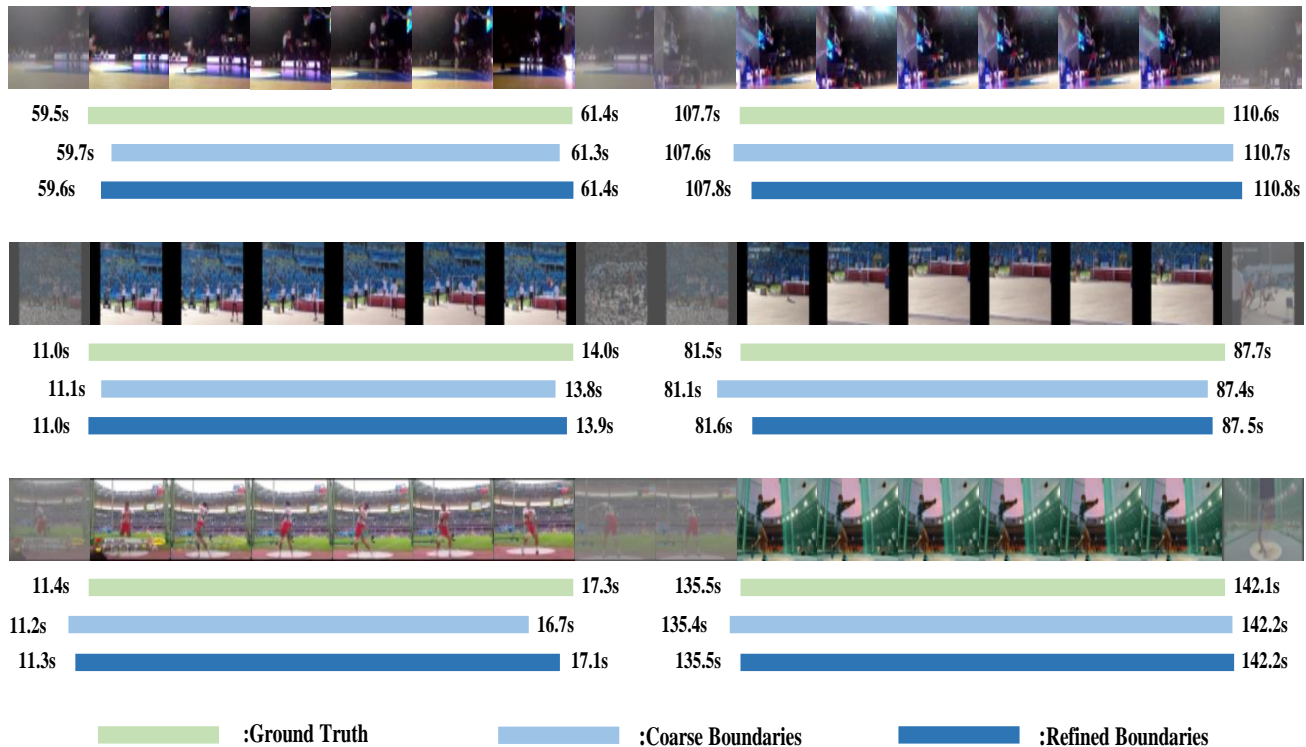


Fig. 5: Visualization examples of the boundaries predicted by the proposed TAL-MTS on THUMOS14 dataset.

worse when the patch size is 16×16 . Because the distinction between foreground action and background is not obvious enough in some patches, thus, the features of these patches will be mistaken for the background to affect the separation of foreground action and background. Thus, a suitable patch size can enhance foreground action information and better separate foreground actions and background noises. Finally, the patch size is set to 24×24 and the $Avg\{0.3 : 0.7\}$ is 54.2%.

D. Impact of different tIoU thresholds.

For the TAL-MTS method to achieve the best performance, we follow the approach of [48] and [40], and discuss the impact of different tIoU thresholds on the THUMOS14 dataset. As can be seen from Table VII, when the tIoU threshold is 0.2, mAPs of 0.3 and 0.4 achieve the best performance. When the tIoU threshold is 0.5, mAPs of 0.6 and 0.7 achieve the best performance. When the tIoU threshold is 0.3, only mAP of 0.5 achieves the best performance, but the Avg which is 0.15% higher than tIoU threshold of 0.2 and also 0.21% higher than tIoU threshold of 0.5 achieves the best result. Although other tIoU thresholds achieve the best results at different mAPs, we still set the tIoU threshold to 0.3 because it achieves the best performance on average. Setting the tIoU threshold to 0.3 achieves as good performance as possible on all mAPs, which makes the fitting better of the TAL-MTS method better.

E. Visualization prediction boundaries.

In this section, we visualize the comparison between the predicted boundaries of TAL-MTS and the ground truth on the THUMOS14 dataset. Some of the results are shown in

TABLE VII: The impact of different tIoU threshold in Soft-NMS on THUMOS14 dataset.

tIoU threshold	mAPs					Avg
	0.3	0.4	0.5	0.6	0.7	
0.2	70.80	65.12	56.73	45.63	32.10	54.08
0.3	70.50	65.04	56.89	46.03	32.71	54.23
0.4	70.06	64.74	56.72	46.16	33.11	54.16
0.5	69.56	64.37	56.53	46.19	33.29	53.99

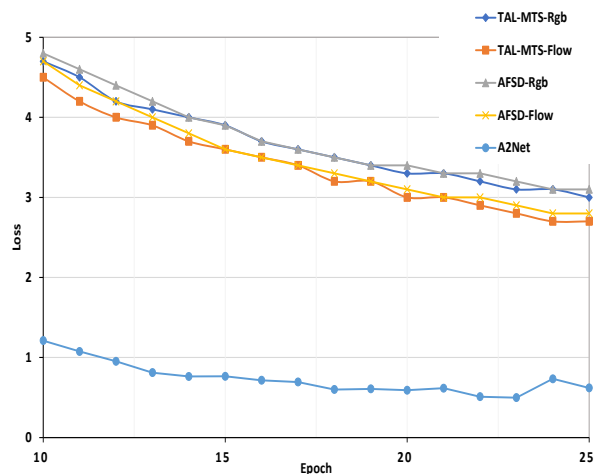


Fig. 6: Loss convergence curves of TAL-MTS on the THUMOS14 dataset, where the x-coordinate denotes the number of epochs, and the y-coordinate indicates the loss values.

Figure 5. The coarse boundaries represent the results without the FSA refinement, and the refined boundaries represent the results after the FSA refinement. We can be seen that although the coarse boundaries are very close to the ground truth, the refined boundaries are more accurate after the FSA refinement. This shows that the FSA model is very effective for TAL-MTS to refine results.

F. Loss convergence analysis.

To further demonstrate the effectiveness of the TAL-MTS method, in this section, we analyze the loss convergence of TAL-MTS on the THUMOS14 dataset and compare it with other anchor-free state-of-the-art methods, such as AFSD [20] and A2Net [48]. As shown in Figure 6, we give the RGB stream and optical-flow stream loss curves of AFSD and TAL-MTS, and also give the loss curve of A2Net. As can be seen from these curves, the TAL-MTS method Whether in the RGB stream or optical-flow stream can converge in 20 – 25 epochs, so the convergence speed is very fast. Compared with AFSD, our method converges faster in both RGB stream, and optical-flow stream, thus, further proving that our method is effective.

VI. CONCLUSION

This paper proposes a novel temporal action localization method with refined features of multi-temporal scales. First, RFP is proposed to obtain refined feature pyramids with stronger semantics information. Then, STT is designed to fully excavate the long-range dependencies of video frames. By combining the two modules, features of multi-temporal scales can be generated. Finally, we use an FSA module to capture the foreground information of each frame, which can reduce the influence of background noises, and further refine the results of localization and classification. Furthermore, we jointly optimize the three models in the framework. Extensive experiments show that we achieve significant results on the THUMOS14 dataset and comparable results on the ActivityNet1.3 dataset. The results show that TAL-MTS is an effective method in the temporal action localization task.

REFERENCES

- [1] Anurag Arnab, Mostafa Dehghani, Georg Heigold, Chen Sun, Mario Lucic, and Cordelia Schmid. Vivit: A video vision transformer. In *2021 IEEE/CVF International Conference on Computer Vision, ICCV 2021, Montreal, QC, Canada, October 10-17, 2021*, pages 6816–6826, 2021. II, III-B
- [2] Lei Jimmy Ba, Jamie Ryan Kiros, and Geoffrey E. Hinton. Layer normalization. *CoRR*, abs/1607.06450, 2016. III-B
- [3] Yueran Bai, Yingying Wang, Yunhai Tong, Yang Yang, Qiyue Liu, and Junhui Liu. Boundary content graph neural network for temporal action proposal generation. In *Computer Vision - ECCV 2020 - 16th European Conference, Glasgow, UK, August 23-28, 2020*, pages 121–137, 2020. II
- [4] Navaneeth Bodla, Bharat Singh, Rama Chellappa, and Larry S. Davis. Soft-nms - improving object detection with one line of code. In *IEEE International Conference on Computer Vision, ICCV 2017, Venice, Italy, October 22-29, 2017*, pages 5562–5570, 2017. III-D, IV-B
- [5] Nicolas Carion, Francisco Massa, Gabriel Synnaeve, Nicolas Usunier, Alexander Kirillov, and Sergey Zagoruyko. End-to-end object detection with transformers. In *Computer Vision - ECCV 2020 - 16th European Conference, Glasgow, UK, August 23-28, 2020, Proceedings, Part I*, pages 213–229, 2020. II
- [6] João Carreira and Andrew Zisserman. Quo vadis, action recognition? A new model and the kinetics dataset. In *2017 IEEE Conference on Computer Vision and Pattern Recognition, CVPR 2017, Honolulu, HI, USA, July 21-26, 2017*, pages 4724–4733, 2017. III-B, IV-C
- [7] Shuning Chang, Pichao Wang, Fan Wang, Hao Li, and Jiashi Feng. Augmented transformer with adaptive graph for temporal action proposal generation. *CoRR*, abs/2103.16024, 2021. II
- [8] Yu-Wei Chao, Sudheendra Vijayanarasimhan, Bryan Seybold, David A. Ross, Jia Deng, and Rahul Sukthankar. Rethinking the faster R-CNN architecture for temporal action localization. In *2018 IEEE Conference on Computer Vision and Pattern Recognition, CVPR 2018, Salt Lake City, UT, USA, June 18-22, 2018*, pages 1130–1139, 2018. I, II, I, II
- [9] Guo Chen, Yin-Dong Zheng, Limin Wang, and Tong Lu. DCAN: improving temporal action detection via dual context aggregation. In *Proceedings of the AAAI Conference on Artificial Intelligence*, 2022. I
- [10] Rui Dai, Srijan Das, Kumara Kahatapitiya, Michael S Ryoo, and Francois Bremond. Ms-tct: Multi-scale temporal convtransformer for action detection. In *Proceedings of the IEEE/CVF Conference on Computer Vision and Pattern Recognition*, pages 20041–20051, 2022. II
- [11] Alexey Dosovitskiy, Lucas Beyer, Alexander Kolesnikov, Dirk Weissenborn, Xiaohua Zhai, Thomas Unterthiner, Mostafa Dehghani, Matthias Minderer, Georg Heigold, Sylvain Gelly, Jakob Uszkoreit, and Neil Houlsby. An image is worth 16x16 words: Transformers for image recognition at scale. In *9th International Conference on Learning Representations, ICLR 2021, Virtual Event, Austria, May 3-7, 2021*, 2021. II, III-C
- [12] Jiyang Gao, Zhenheng Yang, and Ram Nevatia. Cascaded boundary regression for temporal action detection. In *British Machine Vision Conference 2017, BMVC 2017, London, UK, September 4-7, 2017*, 2017. I
- [13] Jiyang Gao, Zhenheng Yang, Chen Sun, Kan Chen, and Ram Nevatia. TURN TAP: temporal unit regression network for temporal action proposals. In *IEEE International Conference on Computer Vision, ICCV 2017, Venice, Italy, October 22-29, 2017*, pages 3648–3656, 2017. I, II, I
- [14] Ross B. Girshick. Fast R-CNN. In *2015 IEEE International Conference on Computer Vision, ICCV 2015, Santiago, Chile, December 7-13, 2015*, pages 1440–1448, 2015. III-D
- [15] Fabian Caba Heilbron, Victor Escorcia, Bernard Ghanem, and Juan Carlos Nibbles. Activitynet: A large-scale video benchmark for human activity understanding. In *IEEE Conference on Computer Vision and Pattern Recognition, CVPR 2015, Boston, MA, USA, June 7-12, 2015*, pages 961–970, 2015. IV-A, IV-A
- [16] Y.-G. Jiang, J. Liu, A. Roshan Zamir, G. Toderici, I. Laptev, M. Shah, and R. Sukthankar. THUMOS challenge: Action recognition with a largenumber of classes. 2014. IV-A, IV-A
- [17] Diederik P. Kingma and Jimmy Ba. Adam: A method for stochastic optimization. In *3rd International Conference on Learning Representations, ICLR 2015, San Diego, CA, USA, May 7-9, 2015, Conference Track Proceedings*, 2015. IV-B
- [18] Hei Law and Jia Deng. Cornernet: Detecting objects as paired keypoints. In *Computer Vision - ECCV 2018 - 15th European Conference, Munich, Germany, September 8-14, 2018*, pages 765–781, 2018. II
- [19] Chuming Lin, Jian Li, Yabiao Wang, Ying Tai, Donghao Luo, Zhipeng Cui, Chengjie Wang, Jilin Li, Feiyue Huang, and Rongrong Ji. Fast learning of temporal action proposal via dense boundary generator. In *The Thirty-Fourth AAAI Conference on Artificial Intelligence, AAAI 2020*, pages 11499–11506, 2020. I, I
- [20] Chuming Lin, Chengming Xu, Donghao Luo, Yabiao Wang, Ying Tai, Chengjie Wang, Jilin Li, Feiyue Huang, and Yanwei Fu. Learning salient boundary feature for anchor-free temporal action localization. In *IEEE Conference on Computer Vision and Pattern Recognition, CVPR 2021, virtual, June 19-25, 2021*, pages 3320–3329, 2021. I, II, III, III-B, III-C, III-C, III-D, IV-B, I, II, III, V, V-F
- [21] Tianwei Lin, Xiao Liu, Xin Li, Errui Ding, and Shilei Wen. BMN: boundary-matching network for temporal action proposal generation. In *2019 IEEE/CVF International Conference on Computer Vision, ICCV 2019, Seoul, Korea (South), October 27 - November 2, 2019*, pages 3888–3897, 2019. I, II, I, II
- [22] Tianwei Lin, Xu Zhao, and Zheng Shou. Single shot temporal action detection. In *Proceedings of the 2017 ACM on Multimedia Conference, MM 2017, Mountain View, CA, USA, October 23-27, 2017*, pages 988–996, 2017. II, I
- [23] Tianwei Lin, Xu Zhao, and Haisheng Su. Joint learning of local and global context for temporal action proposal generation. *IEEE Trans. Circuits Syst. Video Technol.*, 30:4899–4912, 2020. II

- [24] Tianwei Lin, Xu Zhao, Haisheng Su, Chongjing Wang, and Ming Yang. BSN: boundary sensitive network for temporal action proposal generation. In *Computer Vision - ECCV 2018 - 15th European Conference, Munich, Germany, September 8-14, 2018, Proceedings, Part IV*, pages 3–21, 2018. I, II, I, II
- [25] Tsung-Yi Lin, Priya Goyal, Ross B. Girshick, Kaiming He, and Piotr Dollár. Focal loss for dense object detection. *IEEE Trans. Pattern Anal. Mach. Intell.*, 42:318–327, 2020. III-D
- [26] Fuchen Long, Ting Yao, Zhaofan Qiu, Xinmei Tian, Jiebo Luo, and Tao Mei. Gaussian temporal awareness networks for action localization. In *IEEE Conference on Computer Vision and Pattern Recognition, CVPR 2019, Long Beach, CA, USA, June 16-20, 2019*, pages 344–353, 2019. II, I, II
- [27] Zhilong Ou, Yanmin Luo, Jin Chen, and Geng Chen. Srfnet: selective receptive field network for human pose estimation. *J. Supercomput.*, 78:691–711, 2022. I, II, III, I, V
- [28] Zhiwu Qing, Haisheng Su, Weihao Gan, Dongliang Wang, Wei Wu, Xiang Wang, Yu Qiao, Junjie Yan, Changxin Gao, and Nong Sang. Temporal context aggregation network for temporal action proposal refinement. In *IEEE Conference on Computer Vision and Pattern Recognition, CVPR 2021, virtual, June 19-25, 2021*, pages 485–494, 2021. I, II
- [29] Shaoqing Ren, Kaiming He, Ross B. Girshick, and Jian Sun. Faster R-CNN: towards real-time object detection with region proposal networks. *IEEE Trans. Pattern Anal. Mach. Intell.*, 39:1137–1149, 2017. II
- [30] Hamid Rezaatoughi, Nathan Tsoi, JunYoung Gwak, Amir Sadeghian, Ian D. Reid, and Silvio Savarese. Generalized intersection over union: A metric and a loss for bounding box regression. In *IEEE Conference on Computer Vision and Pattern Recognition, CVPR 2019, Long Beach, CA, USA, June 16-20, 2019*, pages 658–666, 2019. III-D
- [31] Zheng Shou, Jonathan Chan, Alireza Zareian, Kazuyuki Miyazawa, and Shih-Fu Chang. CDC: convolutional-de-convolutional networks for precise temporal action localization in untrimmed videos. In *2017 IEEE Conference on Computer Vision and Pattern Recognition, CVPR 2017, Honolulu, HI, USA, July 21-26, 2017*, pages 1417–1426, 2017. I, I, II, III
- [32] Zheng Shou, Dongang Wang, and Shih-Fu Chang. Temporal action localization in untrimmed videos via multi-stage cnns. In *2016 IEEE Conference on Computer Vision and Pattern Recognition, CVPR 2016, Las Vegas, NV, USA, June 27-30, 2016*, pages 1049–1058, 2016. I, III
- [33] Andrei Stoian, Marin Ferecatu, Jenny Benois-Pineau, and Michel Crucianu. Fast action localization in large-scale video archives. *IEEE Trans. Circuits Syst. Video Technol.*, 26(10):1917–1930, 2016. I
- [34] Haisheng Su, Weihao Gan, Wei Wu, Yu Qiao, and Junjie Yan. BSN++: complementary boundary regressor with scale-balanced relation modeling for temporal action proposal generation. In *Thirty-Fifth AAAI Conference on Artificial Intelligence, AAAI 2021*, pages 2602–2610, 2021. I, II, I, II
- [35] Rui Su, Dong Xu, Lu Sheng, and Wanli Ouyang. PCG-TAL: progressive cross-granularity cooperation for temporal action localization. *IEEE Trans. Image Process.*, 30:2103–2113, 2021. I, II
- [36] Jing Tan, Jiaqi Tang, Limin Wang, and Gangshan Wu. Relaxed transformer decoders for direct action proposal generation. In *2021 IEEE/CVF International Conference on Computer Vision, ICCV 2021, Montreal, QC, Canada, October 10-17, 2021*, pages 13506–13515, 2021. I, II
- [37] Ashish Vaswani, Noam Shazeer, Niki Parmar, Jakob Uszkoreit, Llion Jones, Aidan N. Gomez, Lukasz Kaiser, and Illia Polosukhin. Attention is all you need. In *Advances in Neural Information Processing Systems 30: Annual Conference on Neural Information Processing Systems 2017, December 4-9, 2017, Long Beach, CA, USA*, pages 5998–6008. II, III-B, III-C
- [38] Binglu Wang, Xun Zhang, and Yongqiang Zhao. Exploring sub-action granularity for weakly supervised temporal action localization. *IEEE Trans. Circuits Syst. Video Technol.*, 32(4):2186–2198, 2022. I, I, II
- [39] Chenhao Wang, Hongxiang Cai, Yuxin Zou, and Yichao Xiong. RGB stream is enough for temporal action detection. *CoRR*, abs/2107.04362, 2021. III-B, V
- [40] Hanyuan Wang, Dima Damen, Majid Mirmehdi, and Toby Perrett. Tvnet: Temporal voting network for action localization. In *Proceedings of the 17th International Joint Conference on Computer Vision, Imaging and Computer Graphics Theory and Applications, VISIGRAPP 2022, Volume 5: VISAPP, Online Streaming, February 6-8, 2022*, pages 550–558, 2022. V, V-D
- [41] Lining Wang, Haosen Yang, Wenhao Wu, Hongxun Yao, and Hujie Huang. Temporal action proposal generation with transformers. *CoRR*, abs/2105.12043, 2021. II
- [42] Qiang Wang, Yanhao Zhang, Yun Zheng, and Pan Pan. Rcl: Recurrent continuous localization for temporal action detection. In *Proceedings of the IEEE/CVF Conference on Computer Vision and Pattern Recognition*, pages 13566–13575, 2022. II, I
- [43] Li Xiao, Yufan Luo, Chunlong Luo, Lianhe Zhao, Quanshui Fu, Guoqing Yang, Anpeng Huang, and Yi Zhao. Pbrnet: Pyramidal bounding box refinement to improve object localization accuracy. *CoRR*, abs/2003.04541, 2020. III
- [44] Yuanjun Xiong, Limin Wang, Zhe Wang, Bowen Zhang, Hang Song, Wei Li, Dahua Lin, Yu Qiao, Luc Van Gool, and Xiaoou Tang. CUHK & ETHZ & SIAT submission to activitynet challenge 2016. *CoRR*, abs/1608.00797, 2016. IV-C
- [45] Yuanjun Xiong, Yue Zhao, Limin Wang, Dahua Lin, and Xiaoou Tang. A pursuit of temporal accuracy in general activity detection. *CoRR*, abs/1703.02716, 2017. II, I, II
- [46] Huijuan Xu, Abir Das, and Kate Saenko. R-C3D: region convolutional 3d network for temporal activity detection. In *IEEE International Conference on Computer Vision, ICCV 2017, Venice, Italy, October 22-29, 2017*, pages 5794–5803, 2017. I, II, I, II, III
- [47] Mengmeng Xu, Chen Zhao, David S. Rojas, Ali K. Thabet, and Bernard Ghanem. G-TAD: sub-graph localization for temporal action detection. In *2020 IEEE/CVF Conference on Computer Vision and Pattern Recognition, CVPR 2020, Seattle, WA, USA, June 13-19, 2020*, pages 10153–10162, 2020. I, II, I, II
- [48] Le Yang, Houwen Peng, Dingwen Zhang, Jianlong Fu, and Junwei Han. Revisiting anchor mechanisms for temporal action localization. *IEEE Trans. Image Process.*, 29:8535–8548, 2020. II, III, I, II, V, V-D, V-F
- [49] Runhao Zeng, Wenbing Huang, Chuang Gan, Mingkui Tan, Yu Rong, Peilin Zhao, and Junzhou Huang. Graph convolutional networks for temporal action localization. In *2019 IEEE/CVF International Conference on Computer Vision, ICCV 2019, Seoul, Korea (South), October 27 - November 2, 2019*, pages 7093–7102, 2019. I, II, II, V
- [50] Chen Zhao, Ali K. Thabet, and Bernard Ghanem. Video self-stitching graph network for temporal action localization. In *2021 IEEE/CVF International Conference on Computer Vision, ICCV 2021, Montreal, QC, Canada, October 10-17, 2021*, pages 13638–13647, 2021. I, II
- [51] Peisen Zhao, Lingxi Xie, Chen Ju, Ya Zhang, Yanfeng Wang, and Qi Tian. Bottom-up temporal action localization with mutual regularization. In *Computer Vision - ECCV 2020 - 16th European Conference, Glasgow, UK, August 23-28, 2020*, pages 539–555, 2020. I, II, V
- [52] Yue Zhao, Yuanjun Xiong, Limin Wang, Zhirong Wu, Xiaoou Tang, and Dahua Lin. Temporal action detection with structured segment networks. In *IEEE International Conference on Computer Vision, ICCV 2017, Venice, Italy, October 22-29, 2017*, pages 2933–2942, 2017. II, I, II
- [53] Zixin Zhu, Wei Tang, Le Wang, Nanning Zheng, and Gang Hua. Enriching local and global contexts for temporal action localization. In *2021 IEEE/CVF International Conference on Computer Vision, ICCV 2021, Montreal, QC, Canada, October 10-17, 2021*, pages 13496–13505, 2021. I, II